Title

A new quench detection method for HTS magnets: stray-capacitance change monitoring

Authors

Shen, Tengming

Martchevskii, Maxim

Ravaioli, Emmanuele

et al.

Publication Date

2024-01-21

DOI

10.1088/1402-4896/ab4570/pdf

Peer reviewed

A new quench detection method for HTS magnets: stray-capacitance change monitoring

A new quench detection method for HTS magnets: stray-capacitance change monitoring

E. Ravaioli[1,2], D. Davis[1,3], M. Marchevsky[1], GL. Sabbi[1], T. Shen[1], A. Verweij[2], and K. Zhang[1,4]

[1]Lawrence Berkeley National Laboratory, Berkeley, CA, [2]CERN, Geneva, CH, [3]NHMFL, Tallahassee, FL, [4]Paul Scherrer Institut, Villigen, CH.

E-mail: Emmanuale.Ravaioli@cern.ch

28 February 2019

Abstract. Fast quench detection is a key requirement for the successful implementation of superconducting magnet technology. In high temperature superconductor (HTS) magnets, this issue is especially challenging due to the low quench propagation velocity, and presently represents one of the main factors limiting their application. A new detection technique based on stray-capacitance monitoring is proposed. The capacitance between electrically-insulated magnet elements, such as magnet structure and end parts, is utilized as an indication of local heat deposition in the conductor. In fact, the relative permittivity of helium drops when it changes from the liquid to the gaseous phase. Thus, when heating occurs, part of the helium impregnating the insulation layers boils off, and the monitored stray-capacitance decreases. The proposed technique is successfully demonstrated on three small-scale Bi-2212 magnets manufactured at the Lawrence Berkeley National Laboratory. Results from the detection of thermal runaways and spot-heater induced quenches are reported and discussed. Advantages and limitations of the stray-capacitance method with respect to conventional quench detection methods are assessed.

Keywords: accelerator magnet, high temperature superconductor, quench detection, quench protection, superconducting coil

1. Introduction

Early detection of the quench development is critical for the protection of superconducting magnets. In many practical applications, high-energy density superconducting coils are damaged due to hot-spot overheating if active protection is not timely activated. The most common method for detecting the occurrence of a resistive transition in a low-temperature superconducting coil is voltage monitoring by means of dedicated taps [1, 2].

Fast quench detection in high-temperature superconductor (HTS) magnets is more challenging due to the very low normal zone propagation velocity [3–5]. This feature is

one of the factors currently limiting wider application of HTS magnets. For this reason, various alternative quench detection methods have been explored in the past. These attempts include systems monitoring the voltage across coils magnetically coupled to the protected coil [6, 7], mechanical vibrations [8–13], local variations of magnetization and current distribution [14–20], variation of fiber refraction index with temperature [21–27], or voltage across non-contact capacitive sensors [28, 29].

Recently, we proposed a novel detection method based on monitoring the stray capacitances between magnet-structure elements [30]. The technique was successfully tested on a small-scale, race-track, $Ag/Bi_2Sr_2CaCu_2O_x$ (Bi-2212) magnet manufactured at the Lawrence Berkeley National Laboratory (LBNL) [31]. In this work, we describe in more detail the principles upon which the technique is based and present results from its implementation on two additional magnets, with the aim of further demonstrating and characterizing the proposed method [31, 32].

Magnets often include several metallic elements separated from the coil and from each other by layers of insulation material. Parts of the mechanical structures, supports around which the conductor is wound, and coil-end pieces are examples of such elements. During the transients preceding and following a quench, a number of effects occur, which affect the stray capacitances between the elements and the coil, and between each other. These include:

- local heat deposition, which increases the conductor temperature and causes thermal expansion;
- temperature increase, which affects the insulation material's relative permittivity;
- local changes of temperature, pressure, density, and state of the cryogenic fluid impregnating the insulation layers, which results in a change of its relative permittivity;
- sudden mechanical movements, which can alter the geometry of the coil and the magnet's metallic elements.

The proposed capacitance monitoring technique was implemented on three small-scale, race-track, Bi-2212 magnets manufactured at LBNL [31, 32]. The coils have the same geometry, but different conductor performances and impregnation schemes. The measurement setup and the experimental results will be described and discussed. Furthermore, advantages and limitations of this method will be assessed.

2. Method

The electrical capacitance between two elements is defined as $C{=}q/U$ [F], where $\pm q$ [C] is the electrical charge on the elements, and U [V] the voltage across them. Calculations of C for various geometries have been performed and are available in the literature [33]. A simple example is the capacitance between two plane conductors, which is computed as $C{=}\epsilon_0\epsilon_r S/d$, where $\epsilon_0{\approx}8.854{\cdot}10^{-12}$ F/m is the electric constant, ϵ_r

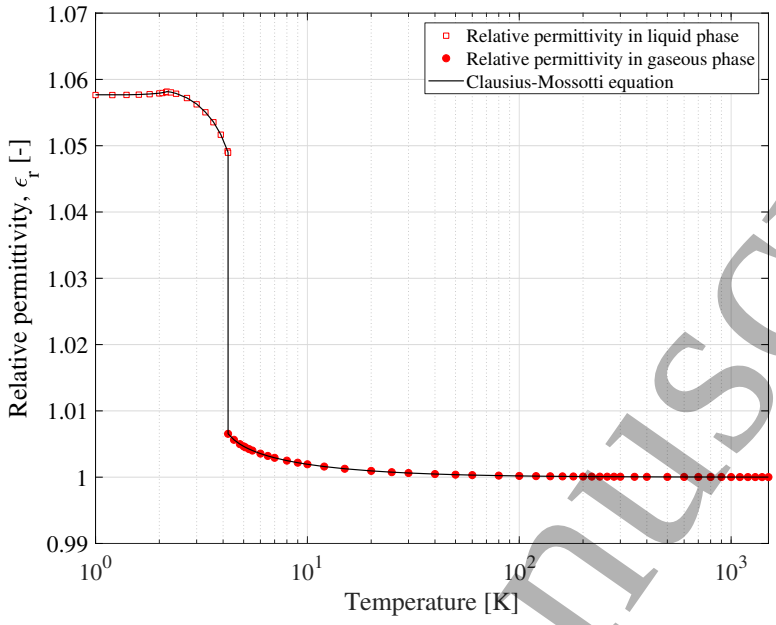

Figure 1. Relative permittivity of helium, measured at atmospheric pressure in liquid and gaseous phases, reported in [34]. The measured permittivity is compared to values calculated with the Clausius-Mossotti equation [34, 36, 37].

the relative permittivity of the material between the conductors, S [m^2] their contact surface, and d [m] the distance between them.

In a superconducting magnet, mechanical, thermal, electrical, and fluid dynamic effects influence C during the transients leading and following a quench. Local conductor heating causes the coil to expand against its structure, whose temperature and dimensions remain almost unaltered during the initial quench development. As a result, the insulation layers between the magnet elements are squeezed, hence reducing d and increasing C. However, no significant size changes are expected for temperatures below about 30 K. Therefore, it is unlikely to observe significant C change due to thermal expansion at the early stage of the quench.

Relative permittivities of the insulation layers and of the cryogenic fluid impregnating them vary with temperature and fluid dynamic conditions. In particular, both helium's and nitrogen's ϵ_r slightly decrease with temperature when in liquid phase, and sharply decrease when their phase changes from liquid to gaseous [34,35]. When heat is locally generated, part or all of the fluid trapped in the insulation layers evaporates, therefore causing a reduction of ϵ_r and consequently C.

Experimental values of helium ϵ_r at atmospheric pressure, available in the literature [34], are shown in Fig. 1. At a temperature of 4.222 K, helium is transferred from the liquid to the gaseous phase and its ϵ_r drops by about 4%. As shown in Fig. 1, this is consistent with the Clausius-Mossotti equation, which relates the relative permittivity of a fluid to its density [36, 37]:

$$\frac{3M}{4\pi}\frac{\epsilon_r - 1}{\epsilon_r + 2}\frac{1}{\rho} = p, \tag{1}$$

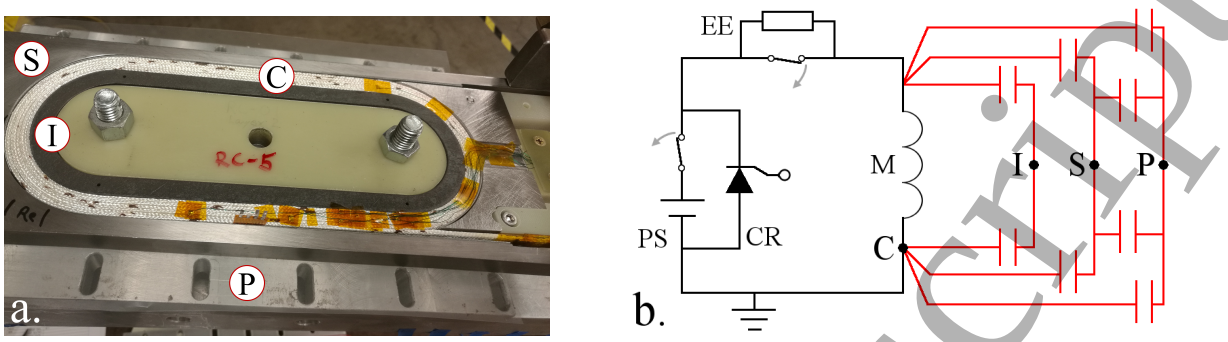

Figure 2. One of the $Ag/Bi_2Sr_2CaCu_2O_x$ racetrack magnets on which the stray capacitance quench detection method is applied [31, 32]. a. Photography showing the coil (C), the pole island (I), the horse-shoe (S), and the plate (P). Half of the plate was removed to show the coil assembly. b. Simplified electrical scheme of the magnet circuit, composed of a power supply (PS), its crowbar (CR), an energy-extraction system (EE), and the magnet (M). Stray capacitances are indicated in red.

where M [g/mol] is the fluid molar mass, ρ [kg/m^3] its density, and p [m^3/kg] its specific polarizability. For helium, $M{\approx}4.003{\cdot}10^{-3}$ kg/mol and $p{\approx}A{+}B\rho$, with $A{=}123.493{\cdot}10^{-6}$ m^3/kg and $B{=}{-}5.86{\cdot}10^{-9}$ m^6/kg^2 [34].

This property can be exploited to detect early heat deposition, which can lead to a quench. Local heat deposition can cause the helium trapped in the insulation layers to evaporate. The local drop of its density causes a reduction of its ϵ_r, and a consequent reduction of the monitored C.

3. Experimental Setup

A series of tests were performed on three small-scale HTS magnets to evaluate the effectiveness of the proposed C monitoring method. The three magnets are made of Bi-2212 superconductor and have the same double-pancake geometry [31, 32].

A picture of one of the magnets, showing the elements composing its structure, is shown in Fig. 2a. The coil (C) turns are wound around an INCONEL® 600 pole island (I), and are kept in place by a stainless-steel plate (P) and so-called horse-shoes (S) at the ends. The metal parts I, S, and P are insulated from the coil and from each other by an additional 120 μm layer of kapton. A simplified electrical scheme of the test magnet circuit, including the stray-capacitances between the magnet elements, is shown in Fig. 2b.

The main magnet and conductor parameters are summarized in Table 1. The conductor is a Rutherford cable composed of 17 strands with a 0.778 mm diameter. Each cable is insulated by a mullite ($2Al_2O_3/SiO_2$) sleeve with an average thickness of 150 μm.

Key differences between the three tested magnets (RC2, RC3, RC5) are highlighted in Table 2. First, their conductor performances are significantly different, following the recent improvement of Bi-2212 critical current [31, 32]. Second, their impregnation

Table 1. Main Magnet and Conductor Parameters [31, 32].

Parameter	Unit	Value
Superconductor	-	Bi-2212
Stabilizer	-	Ag
Insulation	-	Al_2O_3/SiO_2 (Mullite)
Magnetic transfer function	T/A	$407{\cdot}10^{-6}$
Number of layers	-	2
Number of turns per layer	-	6
Approximate total cable length	m	8
Strand diameter, after heat treatment	mm	0.778
Fractions of Ag-0.2wt%Mg, Ag, Bi-2212	-	0.25, 0.50, 0.25
Number of strands	-	17
Cable bare width	mm	7.80
Cable bare height	mm	1.46
Filament twist-pitch	-	Untwisted
Strand twist-pitch	mm	55
Insulation thickness	mm	0.15

Table 2. Main Differences between the Three Tested Magnets.

Magnet	Peak current [A]	Impregnation	Splice losses
RC2 [31]	5782	Beeswax	Not present
RC3 [31]	6485	Epoxy NHMFL mix 61 [38, 39]	Present
RC5 [32]	8284	Epoxy CTD 101k [39–41]	Present

schemes are different. In particular, RC2 was impregnated with beeswax to allow an easier coil examination after the test campaign. Lastly, non-negligible ohmic losses were observed in the splices of RC3 and RC5.

The C measurement system is based on a Keysight E4980AL precision LCR meter. In the selected configuration, the instrument continuously applies a 1 V, 300 kHz, AC voltage across two elements to monitor. With these settings, a new value of C is measured every 90 ms. Both, the LCR meter and one magnet current lead grounded to the main earthing line of the test facility. The magnet transport current I_{m} [A] is mostly unaffected by the applied AC voltage, since the elements I, P, and S are galvanically insulated from the coil.

The six stray capacitances between the four elements C, I, P, and S (see Fig. 2b) were measured in gaseous helium at room temperature, and in a liquid-helium bath with temperature T_{bath}=4.2 K. The values measured for the RC5 magnet are reported in Table 3. The most practical stray capacitance signal to monitor is that between P and S, C_{PS} [F]. In fact, it was considered prudent to avoid connecting directly the C measurement system to the coil during powering tests. Furthermore, C_{PS} is by far the

Table 3. Stray Capacitances Between the Elements of RC5 Magnet Structure, Measured in Gaseous Helium at Room Temperature and in Liquid Helium at T_{bath}=4.2 K, in Units of pF.

Room Temperature	C	P	S	I	Liquid He	C	P	S	I
C	-	1329	1128	260	C	-	1145	976	264
P	-	-	5696	103	P	-	-	5233	109
S	-	-	-	92	S	-	-	-	101

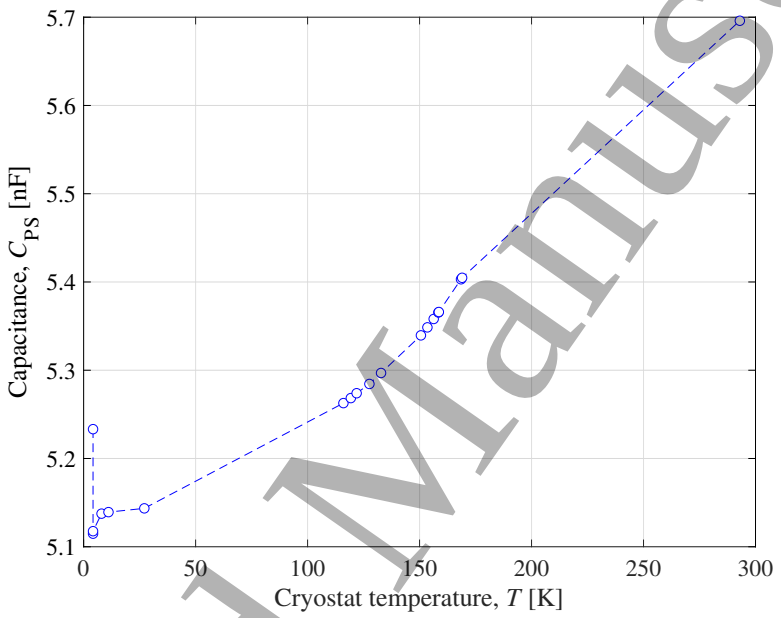

Figure 3. Stray capacitance between the plate and the horse-shoe C_{PS}, versus cryostat temperature, measured during the warm-up of RC5 magnet.

largest of the available C signals, and thus it is easier to measure a change of its value.

3.1. Capacitance Measurement as a Function of Helium Conditions

The C_{PS} measured during the RC5 warm-up is plotted in Fig. 3, as a function of the recorded cryostat temperature. As expected, at the transition between liquid and gaseous phase (T_{bath}=4.222 K), C_{PS} drops due to the helium relative permittivity decrease shown in Fig. 1. When the magnet is surrounded by gaseous helium, from T_{bath}=4.2 K to room temperature C_{PS} increases with the temperature due to thermal expansion. In fact, in first approximation all sizes of the magnet-structure metallic parts increase by a similar coefficient α. Under this simplification, S increases with α^2, while d increases with α.

The difference between C_{PS} in liquid and gaseous helium at T_{bath}=4.2 K, $|\Delta C_{\mathrm{all-gas}}|$, amounts to about 118 pF, i.e. 2.3%. This amount represents the maximum C_{PS} drop that can be observed during the transient leading to a quench, in the extreme case where all helium impregnating the insulation layers between P and S evaporates. In practical

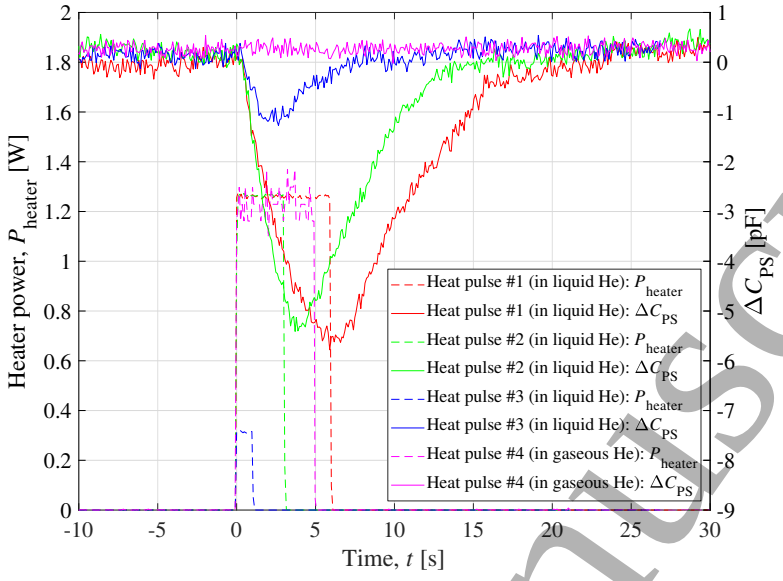

Figure 4. RC5 stray capacitance measurement in presence of local heat deposition. Measured ΔC_{PS} and spot-heater power calculated from the measured heater current ($P_{heater}=R_{heater}I^2_{heater}$, with $R_{heater}=3.6\ \Omega$), versus time. Comparison between tests conducted in liquid and in gaseous helium for various heat-pulse amplitudes and durations.

cases, most heat is deposited in a relatively small volume, and hence only part of the impregnating helium can evaporate before a quench occurs.

3.2. Capacitance Measurement with Local Heat Deposition

The sensitivity of the C monitoring method was assessed by measuring the capacitance change ΔC_{PS} in the presence of local heat deposition. A series of tests was conducted, in which square heat pulses of different amplitudes and durations were applied to a 10 mm long heater strip located between the coil outer insulation and the horse-shoe piece.

The experimental results of four such tests are shown in Fig. 4. An appreciable ΔC_{PS} was measured for heat deposition as low as 0.3 J during heat-pulse tests performed in liquid helium at $T_{bath}=4.2$ K. C_{PS} returned to its original value when the evaporated liquid helium re-impregnated fully the magnet insulation layers. This process took several tens of seconds.

Interestingly, no ΔC_{PS} was observed during the test conducted in gaseous helium. This is expected, since the helium relative permittivity change is minimal in the gaseous phase, as observed in Fig. 1.

4. Calibration of the Stray-Capacitance Monitoring System

The three Bi-2212 magnets were tested individually in liquid helium. Their operational quench detection was based on a conventional voltage-tap system, with a voltage threshold of 20 mV (for RC3) or 100 mV (for RC2 and RC5). Simultaneously, the

Table 4. Qualitative Description of Thermal Regimes in HTS Coils.

Regimes	Conductor Temperature	Current	Ohmic Loss
No Transport Current	T=T_{bath}	0	0
Superconducting (SC)	T<T_{cs}	100% in SC	0
Current Sharing	T_{cs}<T<T_{c}	Shared	P_{ohm}<P_{cooling}
Thermal Runaway	T>T_{c}	Shared	P_{ohm}>P_{cooling}

capacitance C_{PS} was monitored to gather additional information about the magnet behavior.

4.1. Current Sharing Regime in Ag/Bi-2212 Coil

In order to better understand the C changes observed during the experiments, the current-sharing regime in the tested coils is briefly described. The four regimes qualitatively characterizing the coil thermal behavior are listed in Table 4. When no current flows in the coil windings, the conductor temperature T [K] is at the equilibrium with T_{bath}. When I_{m}>0, the conductor remains fully superconducting if T is lower than the current-sharing temperature T_{cs} [K]. If T>T_{cs}, part of the current flows through the superconductor (SC), and part through the Ag matrix. Hence, local ohmic loss arises. The magnet remains in this current-sharing regime without quenching if T is lower than the critical temperature T_{c} [K] and if locally the ohmic loss is lower than the cooling of the cryogenic fluid, i.e. P_{ohm}<P_{cooling}. Due to the high stability of the Ag/Bi-2212 conductor, the magnet can be operated in the current-sharing regime for long periods of time, even in the presence of relatively high ohmic loss [31]. When P_{ohm}>P_{cooling}, a thermal runaway occurs, which leads to a fast increase of T and to a quench.

4.2. Stray-Capacitance Monitoring During Powering Tests

In order to investigate the coil behavior at different current levels, the current of magnet RC3 was set to increase following the staircase pattern shown in Fig. 5. The current was brought at different levels between 3.04 kA and 6.25 kA, and held steady for 120 s at each level. The same ramp-rate of dI_{m}/dt=25 A/s was used for all the ramps.

The measured voltage across the coil ΔU [V] during the power test is plotted in Fig. 5. Its signal was digitally filtered using a multi-band notch filter to reduce the noise introduced by the power supply. During each current ramp, a positive inductive voltage develops across the coil, i.e. ΔU>0. During the plateaux, the inductive voltage is not present, and hence if the coil was fully superconducting ΔU would be nil. However, for I_{m} higher than about 5 kA, a non-zero ΔU develops. This indicates that around that current the coil enters the current-sharing transition described in section 4.1, and hence a resistive voltage arises across it. The amplitude of the observed resistive voltage is in the order of tens to hundreds of μV.

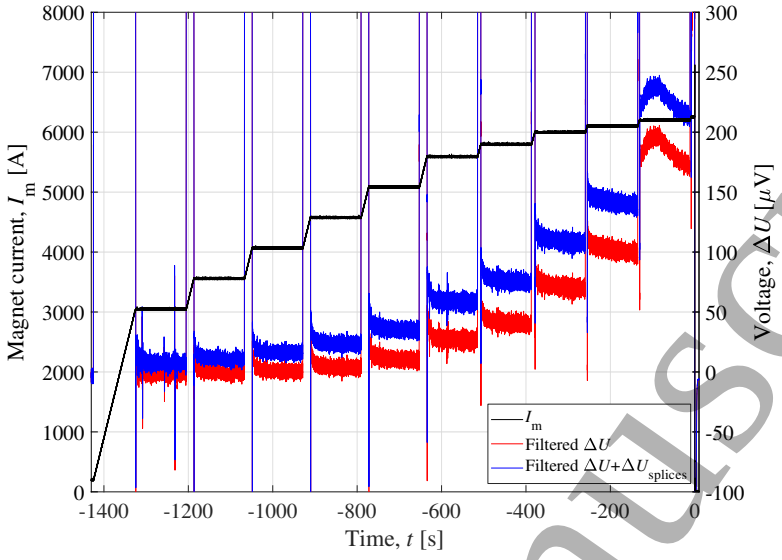

Figure 5. RC3 powering test. Measured magnet current, voltage across the coil, and voltage across coil and its splices, versus time. Voltage signals were digitally filtered to reduce noise.

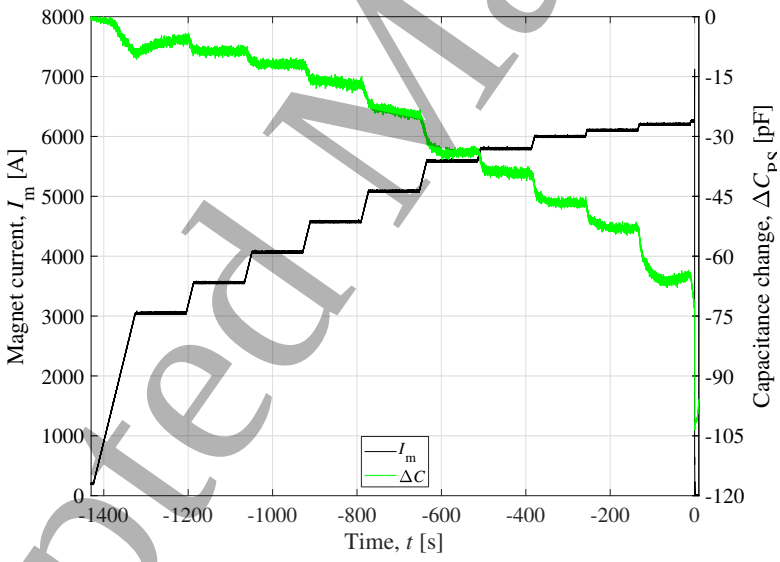

Figure 6. RC3 powering test. Measured magnet current and stray capacitance ΔC_{PS}, versus time.

Furthermore, the measured voltage across the coil and its two splices $\Delta U+\Delta U_{\mathrm{splices}}$ [V] is plotted in Fig. 5. A non-zero $\Delta U_{\mathrm{splices}}$ can be observed at current levels higher than about 3 kA. This indicates that a certain ohmic loss is generated in the splices even before the coil enters the current-sharing regime.

The stray capacitance ΔC_{PS} was monitored during the same powering test, and is plotted in Fig. 6. Whenever heat is locally generated in the coil, a certain amount of helium impregnating the insulation layers evaporates, and a reduction of ΔC_{PS} is observed. In this transient, heat is generated mainly due to three contributions:

coupling loss, ohmic loss in the conductor, and ohmic loss in the splices. Coupling loss occurs during the current ramps due to the magnetic-field change imposed by the transport current variation [42, 43]. For example, the drop of ΔC_{PS} during the first ramp to 3 kA, while no resistive voltage was observed, is due to coupling loss. Note that when the current stops increasing and the coupling loss vanishes, ΔC_{PS} drifts back towards its initial value. Ohmic losses in the conductor and in the splices cause local heat deposition. A balance is reached between ohmic loss and helium cooling a few seconds after I_{m} reaches each new current level. During this condition the temperature distribution in the conductor, and hence the amount of evaporated helium, remain unvaried. Thus, a relatively stable value of ΔC_{PS} can be observed at each current level. A system monitoring the C change is sensitive to all heat depositions, but does not provide information about their sources nor locations.

A thermal runaway occurred about 9 s after reaching the last plateau at I_{m}=6.25 kA. ΔU reached the 20 mV voltage threshold in a few tens of milliseconds after the thermal runaway started due to the fast resistive voltage built-up (see Fig. 5). Simultaneously, a significant drop is visible in the ΔC_{PS} signal, which reaches the value $\Delta C_{\mathrm{all-gas}}$, corresponding to the condition at which all helium impregnating the insulation layers is evaporated. Given the poor time resolution of the C monitoring system, which stores a new data point every 90 ms, it is not clear whether the ΔC_{PS} drop occurs during the thermal runaway, i.e. just before t=0, or after the quench is detected by the voltage-tap system and a fast energy-extraction is triggered. Coupling loss developed during the fast discharge could easily explain the observed ΔC_{PS} drop. Future tests with faster acquisition frequency will allow determining more precisely the moment when the largest ΔC_{PS} drop occurs.

Similar powering tests were performed on the RC2 and RC5 magnets as well. The measured ΔU, $\Delta U+\Delta U_{\mathrm{splices}}$, and ΔC_{PS} at each current level are plotted in Fig. 7. As indicated in Table 2, the three coils are made of superconductors with different performances, and can reach significantly different peak currents. Hence, the current-sharing regime occurs at different current levels.

At higher I_{m}, a larger fraction of the transport current flows through the Ag matrix, and hence higher ohmic loss is locally deposited. As a result, the conductor resistance per unit length and the resistive voltage increase. For each coil, measured voltages and capacitance changes generally exhibit a similar dependence on I_{m}. This occurs because at higher I_{m} the additional heat evaporates a larger amount of the helium impregnating the insulation layers, and the gaseous helium has lower ϵ_{r}.

Note that the ΔU voltages presented here are measured across the entire length of the conductor, which is about 8 m long. Therefore, they are not suitable for deriving the superconductor n-values. The n-value of the RC5 superconductor derived from the highest magnetic-field turn, which is about 14 cm long, is 22 [32].

For each coil, the highest current plotted in Fig. 7 corresponds to the highest current level at which the coil could be operated for 120 s without the occurrence of a thermal runaway. The maximum C change, observed at the highest I_{m}, is defined

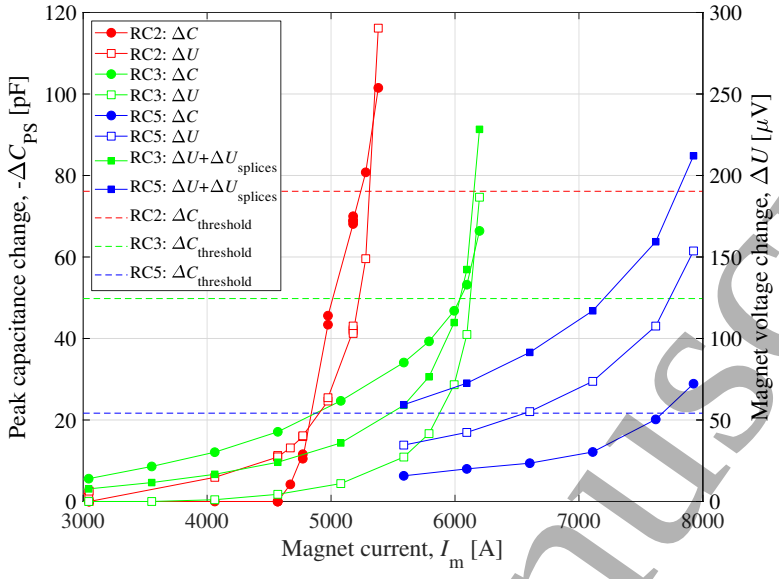

Figure 7. Comparison between measured magnet voltage change across the coil, including the voltage drop across the splices or not, and P-S capacitance change, versus current level. Data obtained from three different Bi-2212 coils in liquid helium at T_{bath}=4.2 K, during 120 s long plateaux at constant current. ΔC thresholds selected for each coil (see Table 5) are indicated with dashed lines. Note that the ΔU voltages presented here are measured across the entire length of the conductor, which is about 8 m, and therefore are not suitable for deriving the superconductor n-values. The n-value of the RC5 superconductor derived from the highest magnetic-field turn, which is about 14 cm long, is 22 [32].

Table 5. Characteristic Stray Capacitance Differences of the Three Tested Magnets.

Magnet	$\lvert\Delta C_{\mathrm{all-gas}}\rvert$ [pF]	$\lvert\Delta C_{\mathrm{max,steady}}\rvert$ [pF]	$\lvert\Delta C_{\mathrm{threshold}}\rvert$ [pF]	Noise of $\lvert\Delta C_{\mathrm{PS}}\rvert$ [pF]
RC2	147	101	76	<1
RC3	111	66	50	<0.3
RC5	124	29	22	<0.05

as $\Delta C_{\mathrm{max,steady}}$ [F]. The values of $\Delta C_{\mathrm{max,steady}}$ for the three coils are reported in Table 5, and compared to the respective $\Delta C_{\mathrm{all-gas}}$ values. RC2 coil's values are higher than for the other coils. This could be explained by the different impregnation scheme: for RC2 beeswax was used, whereas for RC3 and RC5 epoxy was used. Since beeswax is more porous than epoxy, it is expected that a larger amount of helium can penetrate a beeswax-based impregnation, and hence allow for a larger overall C change when evaporation occurs.

The characteristic noise observed on the ΔC_{PS} signal varies considerably between coils. The ratios between the noise and the characteristic $\lvert\Delta C_{\mathrm{max,steady}}\rvert$ are about 1.0%, 0.5%, and 0.2% for the RC2, RC3, and RC5 coils, respectively. Since beeswax is much softer than epoxy, it is expected that higher noise occurs when monitoring the RC2 coil. In fact, in this coil the conductor is not as well maintained in place and local coil

movements can easily lead to C measurement noise. The difference between the noise levels in RC3 and RC5 is presently not fully understood. A possible explanation for this result is the use of different epoxies in the impregnation scheme, as shown in Table 2.

The relatively high noise observed during RC2 tests does not allow a reliable detection of very low heat depositions. This is the reason why ΔC_{PS} shows an appreciable change only above I_{m}=4.6 kA, while ΔU is above zero already at 4 kA.

Monitoring C allows detecting any heat deposition that results in the evaporation of cryogenic fluid impregnating the insulation layers. In the present system, this includes heat deposited in the coil splices. For example, a measurable ΔC_{PS} is observed for RC3 at I_{m} as low as 3 kA. The presence of heating in the splices is confirmed by the measured $\Delta U+\Delta U_{\mathrm{splices}}$. However, no heat is generated in the RC3 superconductor for I_{m}<4.5 kA, and hence $\Delta U\approx 0$.

The tests conducted on the three coils confirm that the proposed C monitoring technique can be used as a means to detect heat deposited in a coil and its splices during the current-sharing regime.

4.3. Selection of Stray-Capacitance Detection Thresholds

In order to implement the method in a quench detection system, a threshold $\Delta C_{\mathrm{threshold}}$ [F] must be selected for the monitored ΔC. Different peak stray-capacitance changes are achieved in the three different coils due to their different characteristics. Thus, a specific threshold need to be set for each individual coil. Here, we propose to select thresholds equal to 75% of $|\Delta C_{\mathrm{max,steady}}|$. The three thresholds, listed in Table 5 and indicated in Fig. 7, are 75 to 440 times higher than their respective noise levels. Thus, they provide a conservative margin with respect to the heat deposition that causes a thermal runaway, while remaining much higher than the noise.

In future implementations of the stray-capacitance detection method, it is envisaged that dedicated capacitive sensors of well-known dimensions and characteristics will be installed on the coil to protect. In that case, the detection threshold will be defined during the design phase, instead of deriving it empirically after powering tests are performed.

The measured ΔC_{PS} at various current levels are plotted in Fig. 8 as a function of the calculated power deposited in the coil, together with the three selected $\Delta C_{\mathrm{threshold}}$. The implemented ΔC monitoring system is sensitive to a deposited heat as low as 25 mW. In comparison, thermal runaway did not start in the coils even in the presence of 1.4 to 1.7 W deposited power. The chosen $\Delta C_{\mathrm{threshold}}$ result in a detection when the deposited heat is about 1 W.

5. Quench Detection with the Stray-Capacitance Monitoring System

The proposed C monitoring system is used to detect thermal runaways occurring in the three tested Bi-2212 magnets in liquid helium at T_{bath}=4.2 K. Various examples of

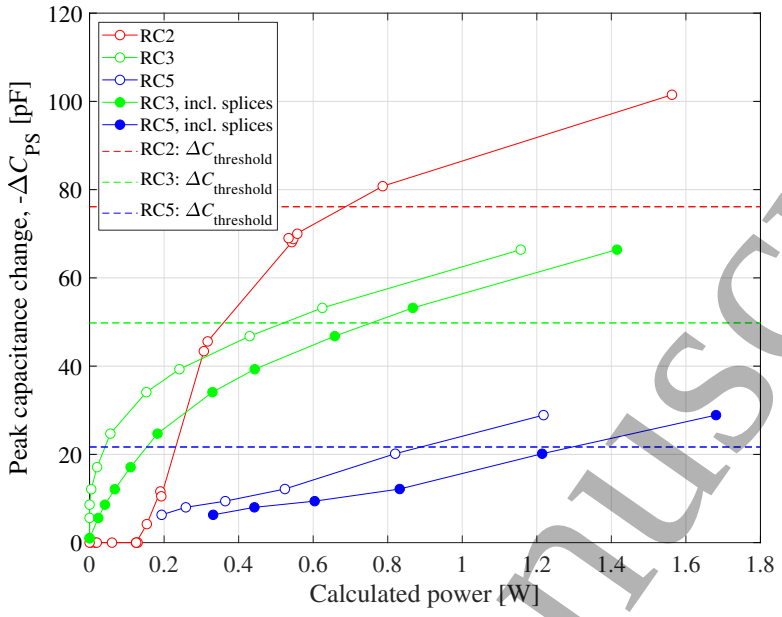

Figure 8. Measured P-S capacitance change versus power deposited in the coil, calculated from measured $\Delta U I_{\mathrm{m}}$ and $(\Delta U + \Delta U_{\mathrm{splices}}) I_{\mathrm{m}}$. Data obtained from three different Bi-2212 coils in liquid helium at T_{bath}=4.2 K, during 120 s long plateaux at constant current. ΔC thresholds selected for each coil (see Table 5) are indicated with dashed lines.

quench detection under different operating scenarios are presented and discussed. The quench tests are of two types: thermal runaways due to ohmic loss in the current-sharing regime, and heater-induced quenches.

5.1. Detection of Thermal Runaways

When no current flows in a magnet, the stray capacitances return to their unperturbed value. This process usually takes several tens of seconds. The transport current and the P-S stray-capacitance change with respect to its unperturbed value, measured during thermal runaways that occurred in the RC2 coil, are shown in Fig. 9. In each test, I_{m} was ramped up to an intermediate level of 5.1 kA, held for a few seconds, then ramped to a higher level, and finally held until thermal runaway occurred. During the last step, the current was held for about 20.1, 8.1, and 3.2 s at 5.43, 5.48, and 5.58 kA before a quench occurred, respectively [30]. The higher the current level, the higher the ohmic loss, and the faster a runaway occurred.

When approaching the current level at which thermal runaway occurs, ΔC_{PS} changes significantly. It can be easily verified that ΔC_{PS} is not proportional to I_{m}, nor its time derivative. Hence, it is highly unlikely that the observed C change is an artefact due to ground loops or inductive pick-ups. Furthermore, ΔC_{PS} is not proportional to I_{m}^2, which rules out electro-mechanical forces as the main cause of the observed C change.

ΔC_{PS} reached its threshold 18, 9, and 3 s before the thermal runaway actually occurred, respectively. During the same transients, the measured ΔU remained below

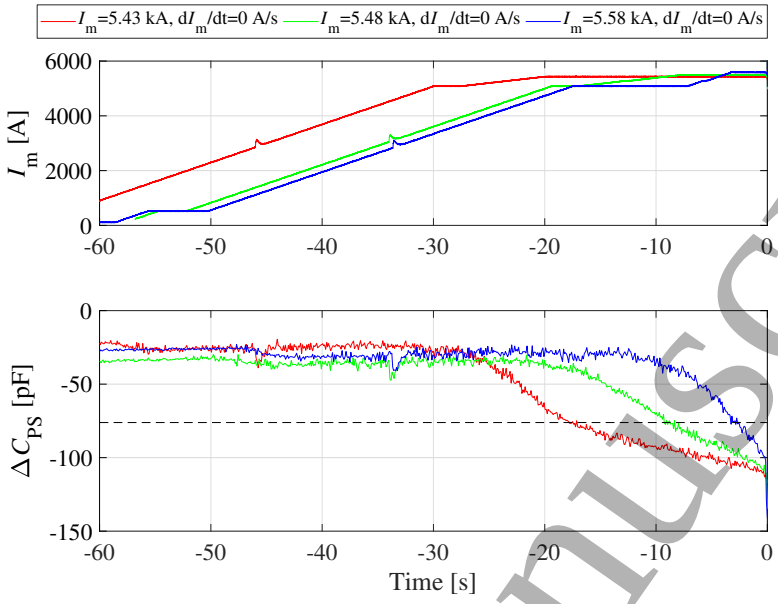

Figure 9. Thermal runaway detection in RC2 coil in liquid helium at T_{bath}=4.2 K, using the proposed stray-capacitance monitoring system. Measured transport current (upper plot) and P-S capacitance change (lower plot) versus time. The proposed detection threshold $\Delta C_{\mathrm{threshold}}$ is indicated with a black dashed line. Quenches occurred while holding I_{m} at different current levels.

1 mV until about 2 s before the runaway, and increased from about 10 mV to the 100 mV threshold during the last 200 ms before the thermal runaway. In all transients analyzed in the rest of the paper, t=0 corresponds to the time at which the voltage-tap based quench detection system was triggered.

For the same current level, ΔC_{PS} reached lower values than those measured during 120-s-long current plateaux in the range of 5.1 to 5.4 kA, previously shown in Fig. 7. This is explained by the fact that during these faster transients the magnet does not dwell at each current level, and hence significantly less ohmic loss in current-sharing regime is deposited. As a result, less helium is boiled off, and lower $|\Delta C_{\mathrm{PS}}|$ is reached.

This result leads to the observation that ΔC_{PS} does not only depend on the instantaneous heat (power) dissipated in the coil, but also on the total heat generated and evacuated by helium during the transient (energy). The same conclusion is reached when comparing thermal runaways occurred during current ramp-ups with different ramp-rates. I_{m} and ΔC_{PS} measured during three such transients are shown in Fig. 10. When ramping up with higher dI_{m}/dt, less ohmic heat is generated to reach the same current level. In fact, in this condition the magnet spends a shorter time at high current, when ohmic loss in current sharing regime is high. Thus, lower $|\Delta C_{\mathrm{PS}}|$ is reached at the moment of the thermal runaway. The $\Delta C_{\mathrm{threshold}}$ was reached 17 s, 1 s, and 30 ms before the thermal runaway for a dI_{m}/dt of 9, 91, and 140 A/s, respectively. The observation that lower heat is deposited in the coil during higher dI_{m}/dt ramp-ups is also sustained by the fact that higher peak current was reached for higher dI_{m}/dt [31].

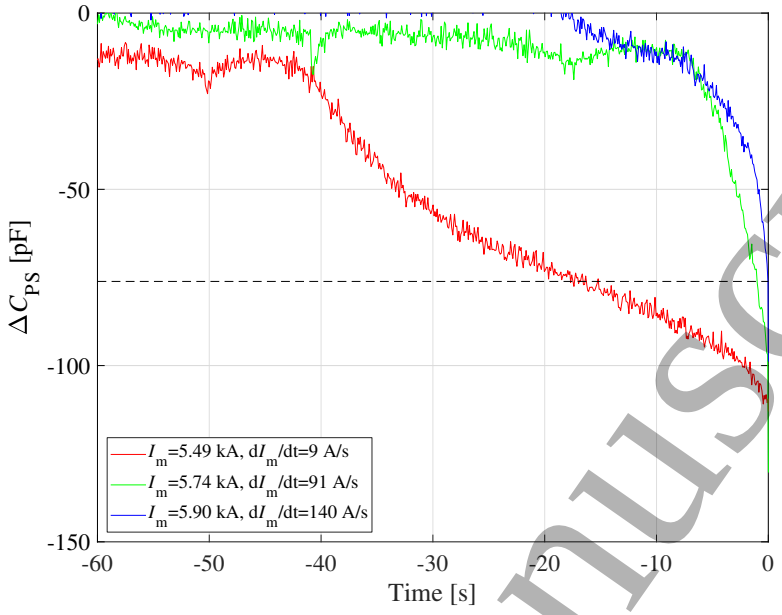

Figure 10. Thermal runaway detection in RC2 coil in liquid helium at T_{bath}=4.2 K, using the proposed stray-capacitance monitoring system. Measured P-S capacitance change versus time. Quenches occurred while ramping I_{m} with different current ramp-rates. The proposed detection threshold $\Delta C_{\mathrm{threshold}}$ is indicated with a dashed line.

Similar tests were conducted on the RC3 magnet, and qualitatively the same results were obtained. I_{m} and ΔC_{PS} measured during five transients leading to thermal runaways are shown in Fig. 11. During two of these transients, I_{m} was ramped up until a quench occurred. The $\Delta C_{\mathrm{threshold}}$ was reached 6 and 0.5 s before the thermal runaway for a dI_{m}/dt of 25 and 128 A/s, respectively. As in the case of RC2, ΔC-based quench detection proved more challenging for higher ramp-rates.

In the other three transients, I_{m} was held for several tens of seconds at a fixed level, and subsequently ramped with dI_{m}/dt=4 A/s until quench. The selected current levels were very close to the highest current at which RC3 can be operated without leading to a thermal runaway, i.e. 6.2 kA. As previously shown in Fig. 7, the magnet can be operated in steady state in the range 5.5 kA$<I_{\mathrm{m}}<$6.2 kA, but a significant resistive voltage develops across it. As a result, ΔC_{PS} changes considerably. The magnet can reach and maintain a steady ΔC_{PS} value if the local ohmic loss is balanced by the helium cooling. However, if the magnet is close to the level at which thermal runaway occurs $|\Delta C_{\mathrm{PS}}|>\Delta C_{\mathrm{threshold}}$. Thus, the selected threshold would prevent operating RC3 during these three transients, as can be observed in Fig. 11. $\Delta C_{\mathrm{threshold}}$ was reached several tens of seconds before the thermal runaway started.

Even earlier detection was achieved during similar tests conducted on the RC5 magnet. The experimental results from five thermal runaways are shown in Fig. 12. The much lower observed noise allows for a noticeably clearer detection of local heating. The selected $\Delta C_{\mathrm{threshold}}$ was reached 2 and 12 s before thermal runaway during ramp-ups

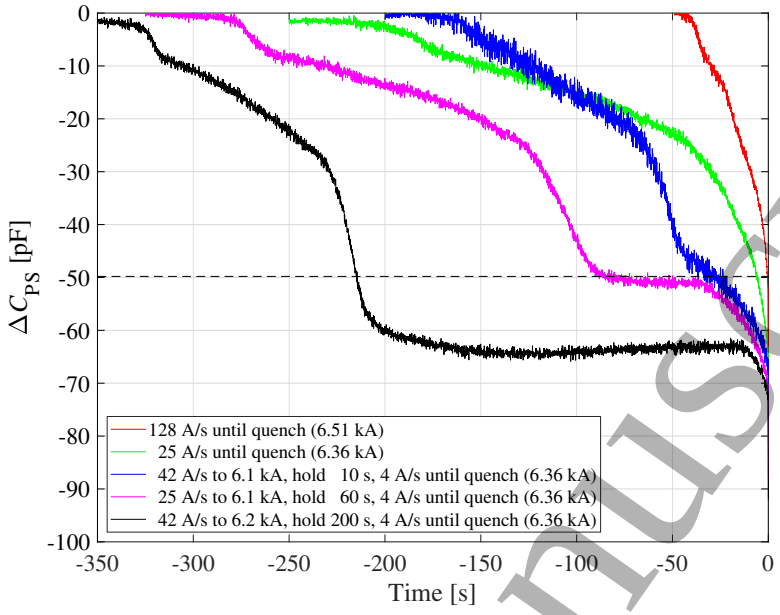

Figure 11. Thermal runaway detection in RC3 coil in liquid helium at T_{bath}=4.2 K, using the proposed stray-capacitance monitoring system. Measured P-S capacitance change versus time. The proposed detection threshold $\Delta C_{\mathrm{threshold}}$ is indicated with a black dashed line. Quenches occurred while submitting I_{m} to different transients, which are described in the legend.

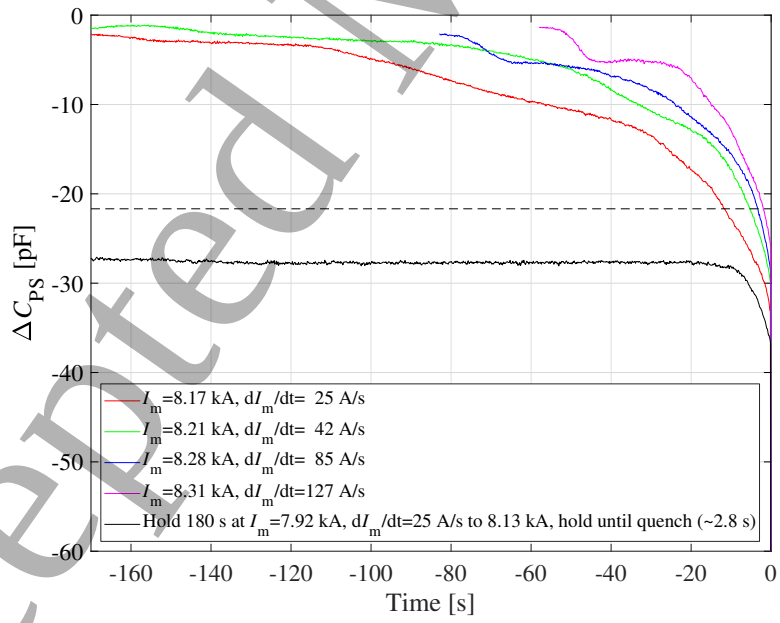

Figure 12. Thermal runaway detection in RC5 coil in liquid helium at T_{bath}=4.2 K, using the proposed stray-capacitance monitoring system. Measured P-S capacitance change versus time. The proposed detection threshold $\Delta C_{\mathrm{threshold}}$ is indicated with a black dashed line. Quenches occurred while ramping I_{m} with different current ramp-rates.

with dI_{m}/dt of 25 and 127 A/s, respectively.

During a different test, the magnet current was held for several minutes at a level of almost 8 kA. As observed in Fig. 7, in this condition the coil is very close to a thermal runway. The chosen $\Delta C_{\mathrm{threshold}}$ would have prevented operating the magnet in this regime, since $|\Delta C_{\mathrm{PS}}|>\Delta C_{\mathrm{threshold}}$. During this transient, more than 1.5 W of ohmic power was constantly deposited in the coil and its splices.

5.2. Detection of Induced Quenches

Additional tests were performed, during which the magnet current was held at a certain level and square heat pulses were applied to a 10 mm long heater strip located between the coil outer insulation and the horse-shoe piece. This allowed investigating the sensitivity of the proposed detection methods to localized heat deposition.

The results of such tests performed on the RC3 magnet are shown in Fig. 13a. Square, 1 s long heat pulses of amplitudes in the range of 0.6 to 22.1 W were introduced until a quench was induced at t=0. ΔC_{PS} visibly changed after each heat pulse was triggered. When local heat was deposited, part of the helium impregnating the insulation layers evaporated, which resulted in a sudden reduction of $\Delta C_{\mathrm{threshold}}$ of several pF, or tens of pF. After each heat pulse, ΔC_{PS} changed back towards the value it had before local heating occurred. This process took several tens of seconds.

At each current level, only the very last heat pulse deposited sufficient heat to start a thermal runaway. However, $\Delta C_{\mathrm{threshold}}$ was reached after each heat pulse. Depending on the application, this high sensitivity to local heat deposition might be desirable or not. On the one hand, it allows early detection of any local heating. On the other hand, it can result in spurious detection if heating occurs without leading to a thermal runaway.

Similar spot-heater tests were performed on the RC5 magnet. The ΔC_{PS} measured during the transients following 1 s long heat pulses of amplitudes in the range of 2.5 to 22.5 W are shown in Fig. 13b. At I_{m}=6.10 kA, all heat pulses caused a reduction of ΔC_{PS} that exceeded $\Delta C_{\mathrm{threshold}}$. At I_{m}=7.92 kA , $|\Delta C_{\mathrm{PS}}|>\Delta C_{\mathrm{threshold}}$ already before introducing any heat pulse.

The results reported in this section indicate that the proposed stray-capacitance monitoring system is sensitive to localized heat depositions, which can potentially lead to a quench.

6. Discussion

The proposed method based on stray-capacitance monitoring was proven to be sufficiently sensitive to effectively detect local heating of the conductor before a quench. The primary mechanism leading to C change was identified as the variation of electrical permittivity of the cryogenic fluid impregnating insulation layers between coil parts. The highest electrical permittivity change occurs when the fluid is transferred from the liquid

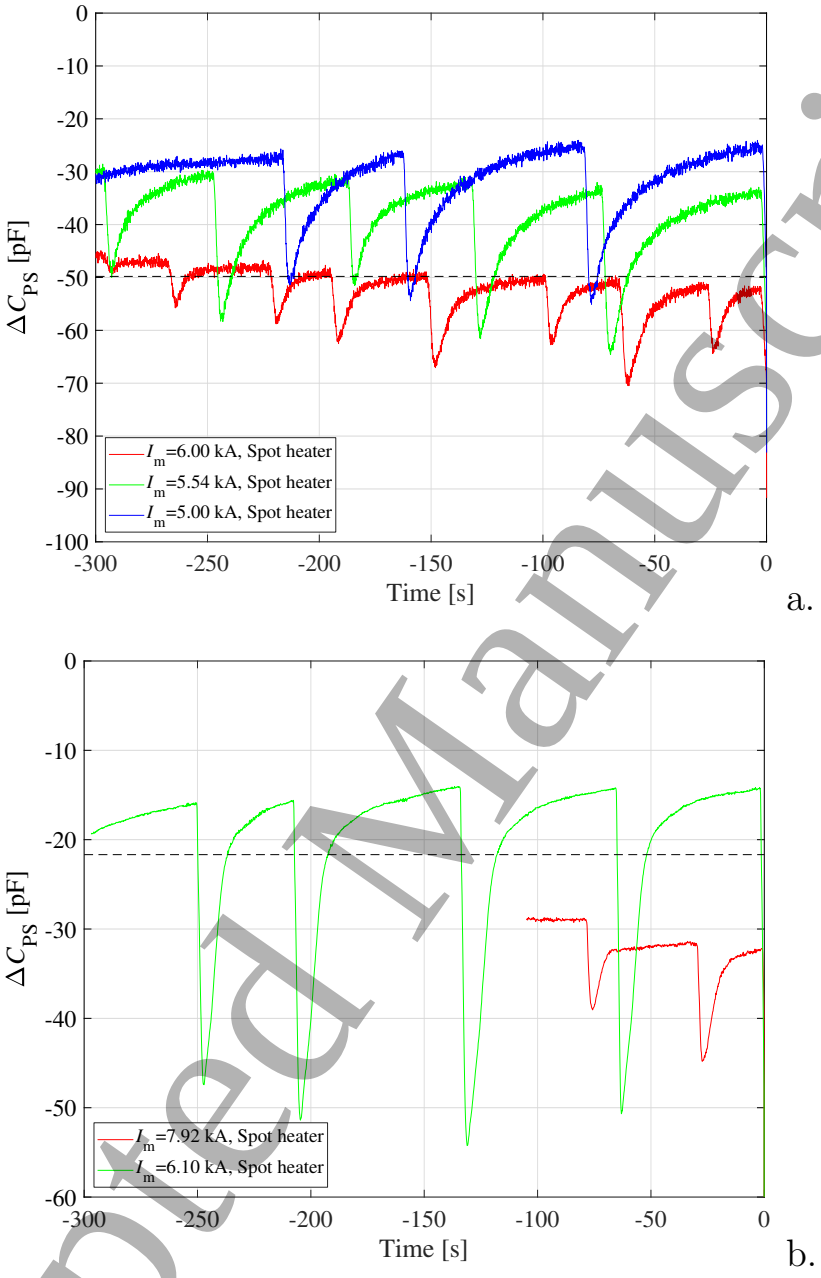

Figure 13. Detection of spot-heater induced quenches in two coils in liquid helium at T_{bath}=4.2 K, using the proposed stray-capacitance monitoring system. Measured P-S capacitance change versus time. Heat pulses of different amplitude and duration were introduced until quench occurred, while I_{m} was held steady. The proposed detection thresholds $\Delta C_{\mathrm{threshold}}$ are indicated with dashed lines. a. RC3 coil. b. RC5 coil.

to the gaseous phase. Thus, in the case of magnets operated in liquid helium, the method is most sensitive to heating increasing the local temperature above 4.222 K. Given the high temperature margin with respect to quench in HTS magnets, it is expected that a significant C change will occur well before the quench occurs.

The early detection of local heating carries advantages and disadvantages. On the one hand, it offers high sensitivity to heat deposited anywhere in the coil and its splices,

which can prevent high continuous cryogenic loss during operation, and ultimately a thermal runaway. Moreover, the monitored signal is independent of the type of heating source. On the other hand, if the local heat deposition is insufficient to start a quench, but sufficient to evaporate part of the helium impregnating the insulation layers, spurious quench detection can be triggered. The observed C change is related to the amount of boiled-off helium, and not directly to the likelihood of a quench.

This monitoring technique is well-suited to be implemented together with the conventional voltage-tap based method. In fact, it relies on a completely different detection mechanism and can offer complementary information about the quench development.

Furthermore, a stray-capacitance detection system can be implemented unobtrusively without any direct electrical connection to the coil to monitor. In the presented configuration, the capacitance between existing magnet-structure elements has been monitored. In future applications, dedicated capacitive detection sensors are envisaged, whose implementation will offer considerable advantages. First, their dimensions and the amount of impregnating helium will be known with greater precision, which in turn will allow a more quantitative definition of the detection threshold. Second, their location can be optimized to improve sensitivity of the method to heating in specific coil positions. Third, they can be constrained more securely, so that mechanical movements and the noise associated with them are reduced.

In the first analysis, it appears the method can be successfully scaled to longer magnets. In fact, the amplitude of the ΔC signal during a quench is affected by the local heating, which is independent of the magnet length. However, the absolute value of C increases for longer magnets, and as a consequence the background noise could increase as well.

The main limitation of the proposed method is the fact that it relies on phase change of the cryogenic fluid. Thus, it cannot be applied for detecting a quench occurring in a magnet operated in gas.

Another shortcoming is the electro-magnetic coupling between the detection system and the magnet electrical circuit, which brings two potential drawbacks. First, electrical perturbations in the magnet circuit can cause C change even in absence of heating. Second, the applied voltage used for monitoring C might introduce a high-frequency noise on the magnet voltage. Both issues will be addressed in future work.

7. Conclusion

A new quench detection method was developed, which utilizes the stray-capacitance change between electrically-insulated magnet elements as an indication of local heat deposition in the conductor. The main mechanism causing the capacitance variation is the change of electrical permittivity of the cryogenic fluid impregnating the insulation layers. A considerable permittivity change occurs when the fluid is transferred from the liquid to the gaseous phase. When heat is locally deposited in the

conductor, part of the fluid impregnating the insulation layers evaporates. Thus, stray-capacitance variation occurs after heating from any source that cause local helium boil-off. The proposed technique is particularly promising for high-temperature superconductor magnets operated in cryogenic liquid. The critical temperature of high-temperature superconductors is well above helium boiling temperature, and thus significant stray-capacitance change is expected before the quench even starts.

The technique was successfully tested on three small-scale $Ag/Bi_2Sr_2CaCu_2O_x$ magnets manufactured at the Lawrence Berkeley National Laboratory. These coils are characterized by a fairly broad current-sharing regime. Hence, they can be operated in liquid helium for tens of seconds at a current level at which ohmic loss constantly occurs. Stray-capacitance change at different magnet current levels was observed, indicating local heat deposition. The presence of a small resistive voltage developed across the coils was confirmed by independent voltage-tap measurements performed during the same tests.

Significant stray-capacitance changes were observed during the transients leading to thermal runaways. For the three coils, capacitance changes higher than the selected detection thresholds occurred seconds, or even tens of seconds, before the quench occurred. Early detection was achieved more easily for ramp-ups with lower ramp-rate, during which more heat was deposited in the coil.

Sensitivity to localized heat deposition was successfully demonstrated by introducing 1 s heat pulses with a 10 mm long spot heater. Stray-capacitance changes above the detection threshold were observed after each heat pulse. An appreciable capacitance change was measured for heat deposition as low as 0.3 J.

The proposed stray-capacitance monitoring method appears a good solution for quench detection in high-temperature superconductor based coils and conductors immersed in cryogenic liquid due to its early heating detection and unobtrusiveness. It does not rely on any direct electrical connection to the coil to protect. It is based on a different physical principle with respect to the conventional voltage-tap quench detection system. Thus, it can be implemented along with voltage taps to provide complementary information about the quench behavior and the coil stability.

A few shortcomings were identified during the first tests of the proposed system. The monitored capacitance can be temporarily perturbed by electro-magnetic transients occurring in the magnet circuit, and drift in time due to variation of the cryogenic conditions. Future developments are considered to address these issues, reduce the noise level, and define more precise detection thresholds. In particular, the implementation of dedicated capacitive sensors of known, controlled dimensions and characteristics, as opposed to utilizing the existing magnet-structure elements, might be particularly beneficial.

Acknowledgments

The authors wish to thank H. Higley, J. Taylor, and M. Turqueti (LBNL) for their help during the coil manufacturing and testing.

Work at LBNL was supported by the Director, Office of Science of the US Department of Energy (DOE) under Contract No. DE-AC02-05CH11231 and also by a US DOE early career award.

K. Zhang acknowledges support from the China Scholarship Council.

D. Davis acknowledges support from the US DOE Office of Science Graduate Student Research Program.

References

[1] J. M. Pfotenhauer, F. Kessler, and M. A. Hilal. Voltage detection and magnet protection. *IEEE Transactions on Applied Superconductivity*, 3(1):273–276, March 1993.

[2] Tengming Shen, Liyang Ye, and Pei Li. Feasible voltage-tap based quench detection in a Ag/Bi-2212 coil enabled by fast 3D normal zone propagation. *Superconductor Science and Technology*, 29(8):08LT01, 2016.

[3] R.H. Bellis and Y. Iwasa. Quench propagation in high tc superconductors. *Cryogenics*, 34(2):129–144, 1994.

[4] F Trillaud, H Palanki, U.P Trociewitz, S.H Thompson, H.W Weijers, and J Schwartz. Normal zone propagation experiments on HTS composite conductors. *Cryogenics*, 43(3):271–279, 2003.

[5] Xiaorong Wang, A. R. Caruso, M. Breschi, Guomin Zhang, U. P. Trociewitz, H. W. Weijers, and J. Schwartz. Normal zone initiation and propagation in Y-Ba-Cu-O coated conductors with Cu stabilizer. *IEEE Transactions on Applied Superconductivity*, 15(2):2586–2589, June 2005.

[6] S. Song, J. Lee, W. S. Lee, H. Jin, J. Lee, Y. J. Hwang, and T. K. Ko. Quench detection method for HTS coils using electromagnetically coupled coils. *IEEE Transactions on Applied Superconductivity*, 25(3):1–4, June 2015.

[7] Y. O. Kim, H. Yonekawa, Y. Chu, K. P. Kim, I. S. Woo, J. I. Song, H. M. Lee, K. R. Park, H. J. Kim, Y. G. Park, W. S. Lee, J. H. Lee, and Y. M. Kim. Development and experimental evaluation of a prototype of the tf secondary quench detection system for kstar device. *IEEE Transactions on Plasma Science*, 44(9):1758–1762, Sept 2016.

[8] A. Ninomiya, K. Sakaniwa, H. Kado, T. Ishigohka, and Y. Higo. Quench detection of superconducting magnets using ultrasonic wave. *IEEE Transactions on Magnetics*, 25(2):1520–1523, Mar 1989.

[9] H M Kim, K B Park, B W Lee, I S Oh, J W Sim, O B Hyun, Y Iwasa, and H G Lee. A stability verification technique using acoustic emission for an HTS monofilar component for a superconducting fault current limiter. *Superconductor Science and Technology*, 20(6):506, 2007.

[10] K.J. Kim, J.B. Song, J.H. Kim, J.H. Lee, H.M. Kim, W.S. Kim, J.B. Na, T.K. Ko, and H.G. Lee. Detection of AE signals from a HTS tape during quenching in a solid cryogen-cooling system. *Physica C: Superconductivity and its Applications*, 470(20):1883 – 1886, 2010. Proceedings of the 22nd International Symposium on Superconductivity (ISS 2009).

[11] M. Yoneda, N. Nanato, D. Aoki, T. Kato, and S. Murase. Quench detection/protection of an HTS coil by AE signals. *Physica C: Superconductivity and its Applications*, 471(21):1432 – 1435, 2011. The 23rd International Symposium on Superconductivity.

[12] M. Marchevsky, G. Sabbi, H. Bajas, and S. Gourlay. Acoustic emission during quench training of superconducting accelerator magnets. *Cryogenics*, 69:50 – 57, 2015.

[13] M. Marchevsky and S. A. Gourlay. Acoustic thermometry for detecting quenches in superconducting coils and conductor stacks. *Applied Physics Letters*, 110(1):012601, 2017.

[14] D. Leroy, J. Krzywinski, V. Remondino, L. Walckiers, and R. Wolf. Quench observation in LHC superconducting one meter long dipole models by field perturbation measurements. *IEEE Transactions on Applied Superconductivity*, 3(1):781–784, March 1993.

[15] T. Ogitsu, A. Devred, K. Kim, J. Krzywinski, P. Radusewicz, R. I. Schermer, T. Kobayashi, K. Tsuchiya, J. Muratore, and P. Wanderer. Quench antenna for superconducting particle accelerator magnets. *IEEE Transactions on Magnetics*, 30(4):2273–2276, July 1994.

[16] T. Ogitsu, A. Terashima, K. Tsuchiya, G. Ganetis, J. Muratore, and P. Wanderer. Quench observation using quench antennas on RHIC IR quadrupole magnets. *IEEE Transactions on Magnetics*, 32(4):3098–3101, Jul 1996.

[17] S. Jongeleen, D. Leroy, A. Siemko, and R. Wolf. Quench localization and current redistribution after quench in superconducting dipole magnets wound with Rutherford-type cables. *IEEE Transactions on Applied Superconductivity*, 7(2):179–182, June 1997.

[18] K Sasaki, T Ogitsu, N Ohuchi, and K Tsuchiya. Study of quench propagation with quench antennas. *Nuclear Instruments and Methods in Physics Research Section A: Accelerators, Spectrometers, Detectors and Associated Equipment*, 416(1):9–17, 1998.

[19] M. Marchevsky, J. DiMarco, H. Felice, A. R. Hafalia, J. Joseph, J. Lizarazo, X. Wang, and G. Sabbi. Magnetic detection of quenches in high-field accelerator magnets. *IEEE Transactions on Applied Superconductivity*, 23(3):9001005–9001005, June 2013.

[20] M. Marchevsky, A. R. Hafalia, D. Cheng, S. Prestemon, G. Sabbi, H. Bajas, and G. Chlachidze. Axial-field magnetic quench antenna for the superconducting accelerator magnets. *IEEE Transactions on Applied Superconductivity*, 25(3):1–5, June 2015.

[21] J. M. van Oort, R. M. Scanlan, and H. H. J. ten Kate. A fiber-optic strain measurement and quench localization system for use in superconducting accelerator dipole magnets. *IEEE Transactions on Applied Superconductivity*, 5(2):882–885, June 1995.

[22] B. J. Soller, D. K. Gifford, M. S. Wolfe, M. E. Froggatt, M. H. Yu, and P. F. Wysocki. Measurement of localized heating in fiber optic components with millimeter spatial resolution. In *2006 Optical Fiber Communication Conference and the National Fiber Optic Engineers Conference*, pages 3 pp.–, March 2006.

[23] W K Chan, G Flanagan, and J Schwartz. Spatial and temporal resolution requirements for quench detection in (RE)$Ba_2Cu_3O_x$ magnets using Rayleigh-scattering-based fiber optic distributed sensing. *Superconductor Science and Technology*, 26(10):105015, 2013.

[24] F Scurti, S Ishmael, G Flanagan, and J Schwartz. Quench detection for high temperature superconductor magnets: a novel technique based on Rayleigh-backscattering interrogated optical fibers. *Superconductor Science and Technology*, 29(3):03LT01, 2016.

[25] F. Scurti and J. Schwartz. Optical fiber distributed sensing for high temperature superconductor magnets. In *2017 25th Optical Fiber Sensors Conference (OFS)*, pages 1–4, April 2017.

[26] Federico Scurti, Srivatsan Sathyamurthy, Martin Rupich, and Justin Schwartz. Self-monitoring 'SMART' (Re)$Ba_2Cu_3O_{7-x}$ conductor via integrated optical fibers. *Superconductor Science and Technology*, 30(11):114002, 2017.

[27] Federico Scurti, John McGarrahan, and Justin Schwartz. Effects of metallic coatings on the thermal sensitivity of optical fiber sensors at cryogenic temperatures. *Opt. Mater. Express*, 7(6):1754–1766, Jun 2017.

[28] N. Nanato and K. Nishiyama. Non-destructive detection of normal transitions in high temperature superconducting coil. *Physics Procedia*, 58:260–263, 2014. Proceedings of the 26th International Symposium on Superconductivity (ISS 2013).

[29] N. Nanato and K. Nishiyama. Locating of normal transitions in a Bi2223 high temperature superconducting coil by non-contact voltage measurement method. *Cryogenics*, 72:53–56, 2015.

[30] E. Ravaioli, M. Martchevsky, G. Sabbi, T. Shen, and K. Zhang. Quench detection utilizing stray capacitances. *IEEE Transactions on Applied Superconductivity*, 28(4):1–5, June 2018.

[31] Kai Zhang, Hugh Higley, Liyang Ye, Steve Gourlay, Soren Prestemon, Tengming Shen, Ernesto Bosque, Charles English, Jianyi Jiang, Youngjae Kim, Jun Lu, Ulf Trociewitz, Eric Hellstrom,

and David Larbalestier. Tripled critical current in racetrack coils made of Bi-2212 Rutherford cables with overpressure processing and leakage control. *Superconductor Science and Technology*, 31(10):105009, 2018.

[32] Tengming Shen, Ernesto Bosque, Daniel Davis, Jianyi Jiang, Marvis White, Kai Zhang, Hugh Higley, Marcos Turqueti, Yibing Huang, Hanping Miao, Ulf Trociewitz, Eric Hellstrom, Jeffrey Parrell, Andrew Hunt, Stephen Gourlay, Soren Prestemon, and David Larbalestier. Stable, predictable and training-free operation of superconducting Bi-2212 Rutherford cable racetrack coils at the wire current density of 1000 A/mm^2. *Scientific Reports*, 9(1):10170, 7 2019.

[33] Yu Ya Iossel, ES Kochanov, and MG Strunskii. The calculation of electrical capacitance. Technical report, Foreign Technology Div Wright-Patterson Afb Oh, 1971.

[34] V.D. Arp, R.D. McCarty, and D.G Friend. Thermophysical Properties of Helium-4 from 0.8 to 1500 K with Pressures to 2000 MPa, 1998. NIST Technical Note 1334 (revised).

[35] J. E. Jensen, H. Brechna, R. G. Stewart, and W. A. Tuttle. *Brookhaven National Laboratory selected cryogenic data notebook*. 1980.

[36] O.F. Mossotti. *Discussione analitica sull'influenza che l'azione di un mezzo dielettrico ha sulla distribuzione dell'elettricità alla superficie di più corpi elettrici disseminati in esso*, volume 24 (Part 2) of *Memorie di Matematica e di Fisica della Società Italiana delle Scienze Residente in Modena*. 1850.

[37] R. Clausius. *Die Mechanische Behandlung der Electricität*. Vieweg+Teubner Verlag, Wiesbaden, 1879.

[38] W. D. Markiewicz, I. R. Dixon, Y. M. Eyssa, J. Schwartz, C. A. Swenson, S. Van Sciver, and H. J. Schneider-Muntau. 25 T high resolution NMR magnet program and technology. *IEEE Transactions on Magnetics*, 32(4):2586–2589, July 1996.

[39] Shijian Yin, Diego Arbelaez, James Swanson, and Tengming Shen. Epoxy resins for vacuum impregnating superconducting magnets: A review and tests of key properties. *IEEE Transactions on Applied Superconductivity*, 2018. Submitted for publication.

[40] G. A. Kirby, L. Gentini, J. Mazet, M. Mentink, F. Mangiarotti, J. Van Nugteren, J. S. Murtomki, P. Hagen, F. O. Pincot, N. Bourcey, J. C. Perez, G. De Rijk, E. Todesco, and J. Rysti. Hi-Lumi LHC twin aperture orbit correctors 0.5-m model magnet development and cold test. *IEEE Transactions on Applied Superconductivity*, 28(3):1–5, April 2018.

[41] F. Savary, E. Barzi, B. Bordini, L. Bottura, G. Chlachidze, D. Ramos, S. Izquierdo Bermudez, M. Karppinen, F. Lackner, C. H. Lffler, R. Moron-Ballester, A. Nobrega, J. C. Perez, H. Prin, D. Smekens, G. de Rijk, S. Redaelli, L. Rossi, G. Willering, A. V. Zlobin, and M. Giovannozzi. The 11 T dipole for HL-LHC: Status and plan. *IEEE Transactions on Applied Superconductivity*, 26(4):1–5, June 2016.

[42] M.N. Wilson. *Superconducting Magnets*. Monographs on Cryogenics. Clarendon Press, 1983.

[43] A P Verweij. *Electrodynamics of superconducting cables in accelerator magnets*. PhD thesis, Twente U., Twente, 1995. Presented on 15 Sep 1995.